Fifty Years of the Indonesian Throughflow*

DEBRA TILLINGER AND ARNOLD L. GORDON

Lamont-Doherty Earth Observatory, Columbia University, Palisades, New York

(Manuscript received 12 December 2008, in final form 14 May 2009)

ABSTRACT

Simple Ocean Data Assimilation (SODA) reanalysis data are used to produce a 50-yr record of flow through the Makassar Strait, the primary conduit for the Indonesian Throughflow (ITF). Two time series are constructed for comparison to the flow through the Makassar Strait as observed during 1997–98 and 2004–06: SODA along-channel speed within the Makassar Strait and Pacific to Indian Ocean interocean pressure difference calculated on isopycnal layers from SODA hydrology. These derived time series are compared to the total ITF as well as to the vertical distribution and frequency bands of ITF variability. The pressure difference method displays higher skill in replicating the observed Makassar ITF time series at periods longer than 9 months, particularly within the thermocline layer (50–200 m), the location of maximum flow. This is attributed to the connection between the thermocline layer and large-scale wind forcing, which affects the hydrology of the ITF inflow and outflow regions. In contrast, the surface layer (0–50 m) is more strongly correlated with local wind flow, and it is better predicted by SODA along-channel velocity. The pressure difference time series is extended over the 50-yr period of SODA and displays a strong correlation with ENSO as well as a correlation at the decadal scale with the island rule.

1. Introduction

The Indonesian Throughflow (ITF), the transport of Pacific Ocean water to the Indian Ocean through the Indonesian seas, is the only low-latitude connection between ocean basins. About 80% of the ITF is funneled through the Makassar Strait (Gordon 2005; Gordon and Fine 1996; Gordon et al. 2008), a narrow passageway with a sill depth of nearly 700 m (Gordon et al. 2003), which crosses the equator between Borneo and Sulawesi. Therefore, the Makassar Strait is an appropriate location for measuring the temporal and spatial characteristics of the Pacific inflow that composes the ITF. The other significant inflow path, Lifamatola Passage, transports deeper Pacific water and does not contribute significantly to flow within the thermocline (van Aken et al. 2009).

Observations of the transport through Makassar Strait were obtained during two periods: from December 1996 through July 1998 as part of the Arus Lintas Indonen (ARLINDO) program (Susanto and Gordon 2005) and from January 2004 to December 2006 as part of the International Nusantara Stratification and Transport (INSTANT) program (Gordon et al. 2008; Sprintall et al. 2004). Mooring arrays are expensive to maintain; thus, there have been efforts to calculate at least part of the ITF from other readily available data, either remote sensing measurements (Potemra et al. 1997) or in situ ocean measurements (Meyers 1996). The ITF can be estimated using interocean pressure gradients, which are usually described by sea surface height differences (Wyrtki 1987), and by integrating large-scale winds (Godfrey 1989). If these approaches can produce a time series that is consistent with in situ observations, they can be used to build a multidecadal time series based on archived hydrological data, which is the objective of this study.

2. Previous calculations of ITF from remote data

a. Calculations from interocean pressure gradients

Wyrtki (1987) hypothesized that a pressure gradient between the Pacific and Indian Oceans drives a flow of Pacific water through the Indonesian archipelago into the Indian Ocean. He used the detrended sea level record at Davao, Philippines, to represent the pressure head in

* Lamont-Doherty Earth Observatory Contribution Number 7302.

Corresponding author address: Debra Tillinger, Lamont-Doherty Earth Observatory, 61 Route 9W, Palisades, NY 10964.
E-mail: debrat@ldeo.columbia.edu

DOI: 10.1175/2009JCLI2981.1

the western Pacific Ocean and the sea level in Darwin, Australia, to represent the eastern Indian Ocean. Together, they form a time series of the sea level difference between the Pacific and Indian Oceans relative to an unknown mean difference. Although Wyrtki found a strong El Niño–Southern Oscillation (ENSO) signal in both sea level pressure datasets, the ENSO signal was not evident in the pressure difference time series. Once observational studies and more advanced models became available, it was clear that ENSO is in fact a dominant signal in the ITF (Clark and Liu 1994; Meyers 1996; Potemra et al. 1997). This discrepancy is likely due to the use of Darwin as representative of the Indian Ocean. He noted that it would be preferable to have sea level records from the south coast of Java; however, long-term records were not kept there.

Waworunto et al. (2001) used a combination of bottom pressure data, travel time data from inverted echo sounders, and satellite altimetry data to determine that the throughflow is primarily baroclinic. The study found that a minimum of three layers was required to successfully approximate the throughflow as measured during ARLINDO. This method calculates an upper bound on transport variability, because energy lost resulting from friction and transfer to eddy kinetic energy are not considered.

Meyers (1996) and Meyers et al. (1995) calculated the geostrophic transport of the Indonesian Throughflow relative to 400 m using repeated XBT sections between Java and Australia. The study found a mean ITF of 5 Sv ($1\ \text{Sv} \equiv 10^6\ \text{m}^3\ \text{s}^{-1}$) in the upper 400 m with a strong relationship with ENSO and annual and semiannual signals. It is also noted that the geostrophic transport across the XBT line is influenced by both the ITF and the South Java Current. The study was expanded by Wijffels et al. (2008) to include a 20-yr record of Ekman and geostrophic transport relative to 750 m. Although their transport values through the Makassar are slightly lower than observed values, they hypothesize that the difference may be from the barotropic component of the flow through the Makassar, which is excluded from the geostrophic calculation, and from the interannual variability, which is better resolved in the XBT data than in the observed values from moorings.

Potemra et al. (1997) expand Wyrtki's original concept by including sea level derived by satellite altimetry at additional locations and by using satellite altimetry to determine that sea level. The concept was further expanded (Potemra 2005) by using both concurrent and leading or lagging sea level data. ITF transport estimated from the earlier XBT data described previously (Meyers et al. 1995) between Java and Australia was compared to the Simple Ocean Data Assimilation (SODA) Parallel Ocean Program (POP) 1.2 transport data along a nearby line. A linear relationship between the ITF along the Australia–Java line and sea level, both derived from SODA, was established. That relationship was then applied to Ocean Topography Experiment (TOPEX)/Poseidon sea level height data near the XBT line to compute the ITF. The results were consistent with the SODA model in terms of variability, but they showed a smaller seasonal cycle and did not show a relationship to ENSO.

In the top 200 m, the SODA transport along the XBT line is best captured by a multivariate linear regression of concurrent sea level at Darwin and Davao and a combination of both concurrent and leading sea level south of Java. The concurrent measurements, which are located near the outflow and inflow of the ITF, respectively, indicate local forcing. The 1-month lead at Java is indicative of coastal Kelvin waves that are forced by Indian Ocean equatorial Kelvin waves, forced by the winds of the central Indian Ocean (Potemra et al. 2002). The 1-month lead at Darwin shows evidence of coastal Kelvin waves, which are forced by Rossby waves in the Pacific Ocean (Potemra 1999). The best fit to total transport also used lagged data from Davao. Potemra suggests that the 1-month lag with Davao sea level could be a feedback in which ITF transport affects Pacific winds, which then affect sea level at Davao.

Burnett et al. (2003) and Kamenkovich et al. (2003) wrote a two-part study of the relationship between the interocean pressure gradient and the ITF. They found a qualitative relationship between the Pacific to Indian Ocean pressure head and the throughflow, but they limited their definition of pressure head to only the sea surface height difference. They deliberately used a barotropic model to better explore the effects of bottom topography but acknowledged that the flow was strongly baroclinic, especially in the Makassar Strait. Within that model, they found that the sea surface height difference did not uniquely determine the total transport of the ITF. They showed that the total transport depends not only on sea surface difference but also on bottom form stress and transports from the Mindanao Current, North Equatorial Counter Current, and New Guinea Coastal Current.

Further support of the necessity of using other pressure data in addition to sea surface height comes from Song (2006). This study combines geostrophic and hydraulic control theories by using sea surface height and ocean bottom pressure data. This method would ideally use ocean bottom pressure data derived from Gravity Recovery and Climate Experiment (GRACE) satellite measurements of the gravity field over the ocean, but because those data were not yet available it used a model-derived proxy. Song determined that using a combination of sea surface height and ocean bottom pressure yielded a

better approximation of ITF variability than either data source alone.

b. Calculations from large-scale winds

The relationship between large-scale winds and flow around an island was first quantified by Godfrey (1989). He developed the ''island rule,'' which explicitly specifies circulation around an island in terms of wind stress. The wind stress is integrated along a path from the western edge of the island across the ocean basin to the eastern boundary of that ocean basin. In the case of the ITF, the island rule is calculated by integrating the wind stress around a line following the western coast of Australia, going across the Pacific Ocean to the coast of South America and back. He calculated an ITF of 16 Sv using this method and calculated 10–13 Sv by calculating depth-integrated steric height differences. Although the latter method allowed for an analysis of the vertical structure of the flow, the advantage of the island rule is that it produces a transport that is independent of any parameterization and requires only wind stress data to compute the ITF transport.

Wajsowicz (1993) rederived and extended the island rule for application to the ITF by including bottom topography and frictional effects along the eastern boundary. This study notes that, although flow through a wide channel between Australia and Asia would be independent of Indian Ocean conditions, the narrow, shallow channels of the Indonesian seas allow both ocean basins to exert control over the flow via frictional and nonlinear effects.

Humphries and Webb (2008) analyzed the ITF in the Ocean Circulation and Climate Advanced Modelling Project (OCCAM) model run with 6-hourly European Centre for Medium-Range Weather Forecasts (ECMWF) winds from 1992 through 1998. This produced a reasonably realistic total throughflow with a strong annual cycle and a correlation with ENSO. However, like the SODA model, the OCCAM model underestimated the flow through the Makassar Strait and overestimated the flow through the Lombok Strait. They then used the island rule to calculate the throughflow and found good agreement between their model and the island rule on time scales of 1 yr or longer. They found this relationship to be diminished in years with strong El Niño events. To explain this, they suggest that the island rule is based on a steady-state solution that does not include gravity waves or Rossby waves. Therefore, they conclude that the energetic waves generated by El Niño take longer than 1 yr to propagate through the Pacific Ocean. However, they could find no evidence that propagation delays were responsible for the difference in the time series, and they do not further explain these results.

c. The current study

The first objective of this study is to find a simple way to use existing hydrographic reanalysis data to reproduce the ITF variability observed during the ARLINDO and INSTANT periods. The second objective is to determine what forces influence the skill of various estimates of ITF variability. The final objective is to use the method developed for the first objective to create a long-term time series of ITF variability and to analyze that long time series to understand the sources of its variability.

3. Data

a. Observational data

In situ velocity data from the ARLINDO (Susanto and Gordon 2005) and INSTANT (Gordon et al. 2008) observational periods were used. The ARLINDO moorings provide Makassar Strait velocity data for the 20 months from December 1996 to July 1998. The INSTANT moorings provide a 35-month record from January 2004 through November 2006. In both studies, two moorings were located near 3°S, 118°E within the Labani Channel, a 45-km-wide constriction within the Makassar Strait. The ARLINDO moorings had 300-kHz acoustic Doppler current profiler (ADCP) at a nominal depth of 150 m and current meters at 200, 250, 350, and 750 m (western mooring) and at 205, 255, 305, and 755 m (eastern mooring). The INSTANT moorings were similarly designed with ADCPs at a nominal depth of 300 m and current meters at 400 and 700 m, with additional current meters on the western mooring at 200 and 1500 m. The data used in this study are monthly means computed from the processed ADCP time series gridded in 10-m bins. The two studies showed similar results in terms of the structure of the flow but displayed a 27% increase in transport during INSTANT, which may be the result of the strong El Niño event that dominated the ARLINDO period (Gordon et al. 2008).

For both periods, velocity from Makassar Strait ADCP time series was normalized to focus on its variability. Converting from velocity to transport requires assumptions about the width of the boundary layers and the rate at which velocity decays toward the sidewalls. Therefore, all in situ data are reported here as velocity. Where transport is discussed, we assume that the boundary layer effect is constant, because we are comparing only the transport variability.

b. Reanalysis data

Reanalysis data from the SODA version 2.02–2.0.4 (Carton et al. 2000a,b) were used to obtain Makassar Strait velocity and to calculate the interocean pressure

difference. SODA uses Parallel Ocean Processing physics and has a horizontal resolution of 28 km by 44 km on the equator, reducing poleward. It has monthly time coverage from January 1958 through December 2007 and 40 vertical levels. SODA integrates 40-yr ECMWF Re-Analysis (ERA-40) winds until 2000 and Quick Scatterometer (QuikSCAT) winds thereafter. The outputs of SODA used in this study are temperature, salinity, velocity, and wind stress, which are all produced on the same temporal and spatial grid. ITF velocities within SODA were taken from the grid boxes closest to the latitude of the ARLINDO and INSTANT moorings and integrated across the Labani Channel.

SODA shows an average transport of 15 Sv from the Pacific Ocean to the Indian Ocean (Carton and Giese 2008) and with the majority of the transport passing through Lombok Strait. This is not in agreement with observational studies (Gordon et al. 2008). This disagreement may be due in part to the inability of a gridded model to resolve the topographic complexity of the Indonesian Straits. In addition, the quality of reanalysis data is in part a function of the quantity of data integrated, and many more observations have been done within the Pacific and Indian Oceans than in the narrow passages of the Indonesian Straits. However, direct comparisons between SODA output and observations show a high degree of accuracy in both sea level and heat content in the tropical Pacific and Indian Oceans, which are the areas used to calculate pressure difference, as will be discussed later.

4. Methods

Inflow and outflow regions for the ITF were identified (Fig. 1, shaded regions). The inflow and outflow areas were then modified to determine the sensitivity of the results to the particular choice of boundaries (see appendix). Pressure coordinates for each of these regions were calculated based on SODA depth levels and the mean latitudes of each region. Within each region, the temperature and salinity profiles were averaged, providing a single profile in each region for every month. Density profiles were calculated from the temperature and salinity profiles so that pressure could then be interpolated on to regular density intervals. Along each of these isopycnals, pressure from the Indian Ocean boundary was subtracted from pressure at the Pacific boundary:

$$\mathrm{PDIFF} = \sum (P_{\mathrm{Pacific}} - P_{\mathrm{Indian}}). \qquad (1)$$

To estimate the depth of these isopycnals within the Makassar Strait, it was assumed that they occur at approximately the same pressure as they do in the Pacific Ocean. This is because the water in the Makassar Strait has not yet passed through the Banda Sea, where the significant mixing occurs and water mass profiles are changed (Ffield and Gordon 1992; Koch-Larrouy et al. 2007). Therefore, the distribution of density relative to pressure in the Makassar Strait is considered here to be the average distribution of density relative to pressure in the Pacific inflow area. The mean pressure difference is then subtracted from the dataset, yielding a time series of pressure difference anomalies for 10-db layers from 10 db below the surface to 1200 db, the effective Pacific to Indian Ocean sill depth of the Indonesian Seas (Andersson and Stigebrandt 2005; Gordon et al. 2003). The pressure difference is defined as positive when the pressure is greater in the Pacific Ocean than in the Indian Ocean (i.e., when the pressure head would yield throughflow from the Pacific to the Indian Ocean). As was the case with Waworunto et al. (2001), these values should be considered upper limits on the variability, because friction effects and transfer to eddy kinetic energy are not included.

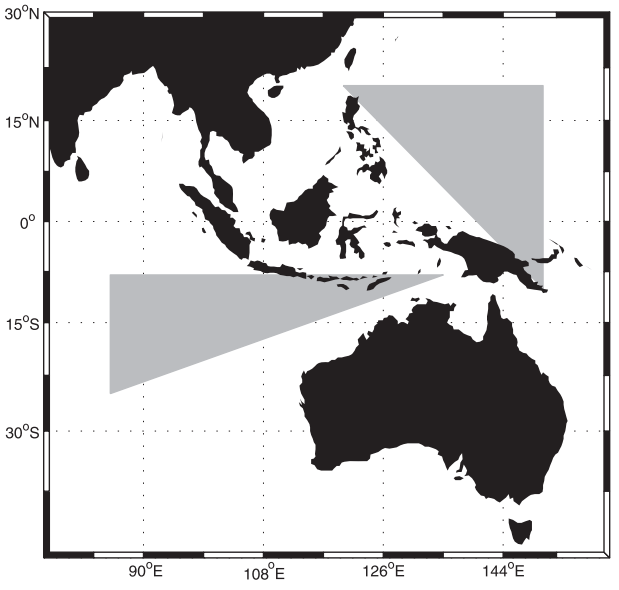

FIG. 1. The shaded areas demarcate the inflow (Pacific Ocean) and outflow (Indian Ocean) regions of the ITF.

To facilitate the comparison of the observed ITF transport variability to the SODA velocities and interocean pressure difference, all time series were normalized to zero mean and unit variance. All statistical results are accurate to within 95% confidence unless otherwise noted.

5. Comparison of time series with in situ data

a. Depth-integrated flow

Our approach provides two SODA-based time series for comparison with the observed in situ data: SODA

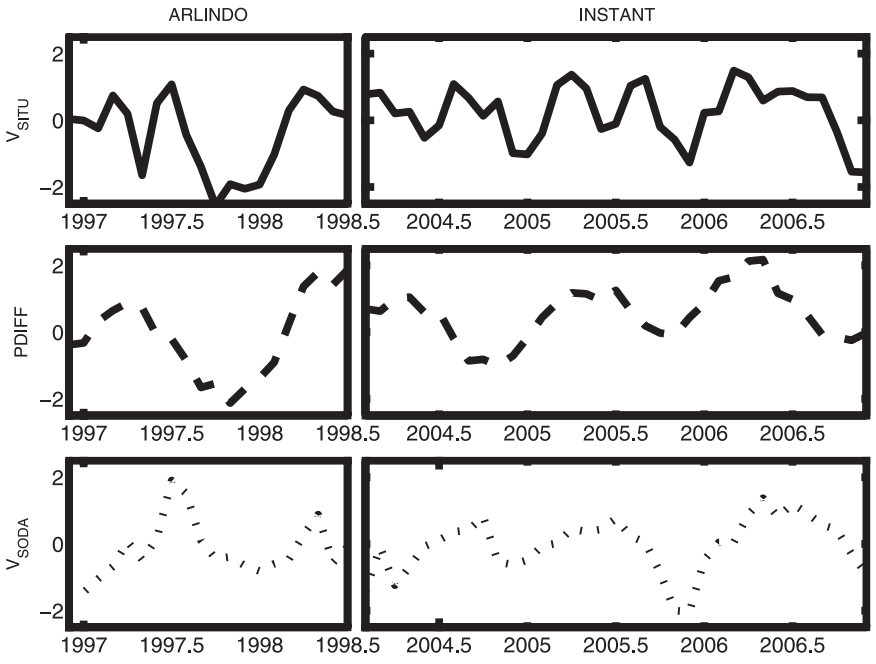

FIG. 2. Variability of (top) $\mathbf{V}_{\mathrm{ARLINDO}}$ and $\mathbf{V}_{\mathrm{INSTANT}}$, (middle) PDIFF, and (bottom) $\mathbf{V}_{\mathrm{SODA}}$.

along-channel velocity $\mathbf{V}_{\mathrm{SODA}}$ and pressure difference calculated from SODA hydrology data (PDIFF). The two in situ datasets, ARLINDO (1996–98) and INSTANT (2004–06), have been normalized relative to their combined variance and mean and have been defined as positive when throughflow is directed from the Pacific to the Indian Ocean. It can be seen in Fig. 2 (left) that ARLINDO velocity $\mathbf{V}_{\mathrm{ARLINDO}}$ has a lower mean but a higher variance than INSTANT velocity $\mathbf{V}_{\mathrm{INSTANT}}$. Both time series have a decorrelation time scale of approximately 3 months.

The correlations between the derived ITF variability and the in situ ITF variability change significantly between the ARLINDO and INSTANT periods (Table 1). During ARLINDO (Fig. 2, left), PDIFF displays higher skill in simulating the monthly variability exhibited by the depth-integrated ARLINDO velocity data $\mathbf{V}_{\mathrm{ARLINDO}}$. SODA along-channel velocity $\mathbf{V}_{\mathrm{SODA}}$ was not significantly correlated with the monthly data during this time. During INSTANT, $\mathbf{V}_{\mathrm{SODA}}$ has the higher predictive skill. The correlation with PDIFF decreases from ARLINDO to INSTANT, although it remains significant.

ARLINDO and INSTANT appear to be representative of two different modes of throughflow variability, each with separate forcings. Although the most apparent reason for the difference in the observational time series is the major El Niño event of 1997 (Gordon et al. 2008), it is helpful to quantify the differences more precisely before discussing the reasons for those differences (section 6). The throughflow is therefore divided in two ways: by pressure layers based on the vertical profile of the throughflow and by frequency bands based on the Fourier transforms of the in situ time series.

b. Depth layers

To further compare the datasets, the flow was first divided spatially into four pressure layers following the division used by Potemra and Schneider (2007). We define the surface layer (SL) as 0–50 db (though approximately the top 10 m of in situ ADCP velocity is considered unreliable because of the nature of ADCP measurements and the instrument depth; RDI 2001). The thermocline layer (TL; 50–200 db) contains the bulk of the transport (Gordon et al. 2008; Susanto and Gordon 2005) and is therefore the main focus of our inquiry. The middle layer (ML; 200–500 db) and the deep layer (DL; 500–1200) contribute little to the total transport. The correlations between the individual layers are shown in Table 2. For these calculations, PDIFF and $\mathbf{V}_{\mathrm{SODA}}$ were each divided into the same four layers as $\mathbf{V}_{\mathrm{ARLINDO}}$ and $\mathbf{V}_{\mathrm{INSTANT}}$.

TABLE 1. Correlation coefficients with p values for the derived time series and in situ data.

	$\mathbf{V}_{\mathrm{ARLINDO}}$		$\mathbf{V}_{\mathrm{INSTANT}}$	
	r value	p value	r value	p value
PDIFF	0.74	0.00	0.41	0.01
$\mathbf{V}_{\mathrm{SODA}}$	0.33	0.15	0.50	0.00

TABLE 2. Correlation coefficients with p values for the derived time series and in situ data within depth layers.

		$\mathbf{V}_{\text{ARLINDO}}$		$\mathbf{V}_{\text{INSTANT}}$	
Layer	Time series	r value	p value	r value	p value
SL	PDIFF	−0.35	0.13	0.05	0.78
(0–50 m)	$\mathbf{V}_{\text{SODA}}$	0.68	0.00	0.41	0.01
TL	PDIFF	0.73	0.00	−0.06	0.75
(50–200 m)	$\mathbf{V}_{\text{SODA}}$	0.42	0.06	0.21	0.23
ML	PDIFF	0.74	0.00	0.43	0.01
(200–500 m)	$\mathbf{V}_{\text{SODA}}$	0.46	0.04	−0.13	0.47
DL	PDIFF	0.54	0.01	0.46	0.01
(500–1200 m)	$\mathbf{V}_{\text{SODA}}$	0.32	0.16	−0.29	0.09

In the SL, which represents the surface mixed layer, PDIFF shows no statistically significant correlation with in situ data during either time period. The TL, which contains most of the ITF transport, shows a very high correlation with PDIFF during ARLINDO but no correlations during INSTANT. This is the largest difference in correlations between the two time periods. In the ML, PDIFF retains its high correlation with $\mathbf{V}_{\text{ARNLINDO}}$ and is also significantly correlated with $\mathbf{V}_{\text{INSTANT}}$. The DL, which contains very little of the transport, is significantly correlated only with PDIFF, with a slightly higher correlation during ARLINDO.

In contrast, $\mathbf{V}_{\text{SODA}}$ does better at predicting the depth-integrated variability (Table 1) during INSTANT than it does during ARLINDO, although is shows more skill at some of the individual layers (Table 2) during ARLINDO as well. Consistently, $\mathbf{V}_{\text{SODA}}$ shows the most skill in the SL, with the highest correlation during ARLINDO, and it is not significantly correlated with the observational data in the TL or the DL during either period but shows a correlation with $\mathbf{V}_{\text{ARLINDO}}$ but not with $\mathbf{V}_{\text{INSTANT}}$ in the ML.

c. *Frequency separation*

A Fourier transform of the two in situ datasets (Fig. 3, top) shows that $\mathbf{V}_{\text{INSTANT}}$ contains more high-frequency power than $\mathbf{V}_{\text{ARLINDO}}$. Power increases with period for $\mathbf{V}_{\text{ARLINDO}}$, suggesting that the 20-month observational period was insufficient to capture a full cycle of variability. That does not appear to be the case for the 35-month $\mathbf{V}_{\text{INSTANT}}$ period, which clearly shows two high peaks, one at 6 months and one at a year. After the annual peak, power decreases with period. Based on $\mathbf{V}_{\text{INSTANT}}$, the variability can be separated into low and high frequencies, defined relative to 9 months. Although the divide is less obvious for $\mathbf{V}_{\text{ARLINDO}}$, a division at 9 months still separates the noticeable 4- and 12-month peaks. During both the ARLINDO and INSTANT time periods, PDIFF is dominated by long-period variability (Fig. 3, middle), and $\mathbf{V}_{\text{SODA}}$ (Fig. 3, bottom) shows power at both short and long periods, with more power in the latter.

A Lanczos filter (Duchon 1979) was used to divide each dataset into periods longer and shorter than 9 months. Correlations between the filtered derived time series and the filtered in situ data can be calculated

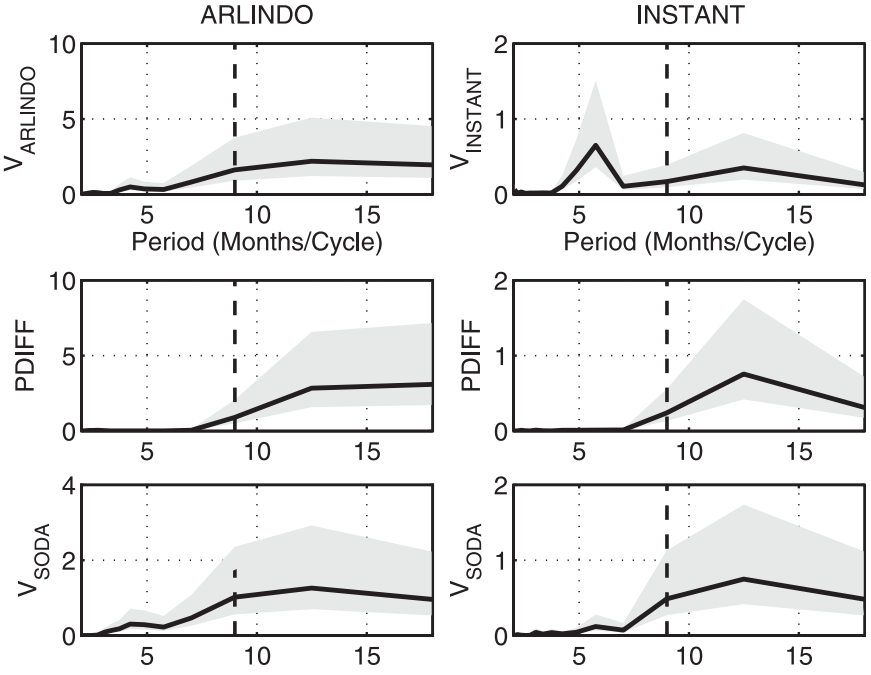

FIG. 3. FFTs of (top) $\mathbf{V}_{\text{ARLINDO}}$ and $\mathbf{V}_{\text{INSTANT}}$, (middle) PDIFF, and (bottom) $\mathbf{V}_{\text{SODA}}$.

TABLE 3. Correlation cofficients with p values for the derived time series and in situ data within frequency bands.

Period	Time series	$\mathbf{V}_{\text{ARLINDO}}$		$\mathbf{V}_{\text{INSTANT}}$	
		r value	p value	r value	p value
Long	PDIFF	0.98	0.00	0.74	0.00
(>9 months)	$\mathbf{V}_{\text{SODA}}$	0.24	0.31	0.79	0.00
Short	PDIFF	−0.17	0.47	−0.01	0.95
(<9 months)	$\mathbf{V}_{\text{SODA}}$	0.57	0.01	0.25	0.15

separately for low and high frequencies (Table 3). When only low frequencies are compared (Fig. 4), PDIFF captures 96% of the variance in $\mathbf{V}_{\text{ARLINDO}}$ and 54% of the variance in $\mathbf{V}_{\text{INSTANT}}$, and $\mathbf{V}_{\text{SODA}}$ fails to capture the variance during ARLINDO but succeeds in capturing 62% of the variance during INSTANT. When only high frequencies are compared (Fig. 5), the only significant correlation is between $\mathbf{V}_{\text{SODA}}$ and $\mathbf{V}_{\text{ARLINDO}}$, which accounts for 32% of the variance.

6. Differences in ocean states between the ARLINDO and INSTANT observational periods

The ARLINDO period was dominated by a strong ENSO event, so it is not surprising that it is comparatively easy to predict its low-frequency variability given the known relationship between the strength of the ITF and ENSO (Gordon and Fine 1996; Humphries and Webb 2008; Meyers 1996). INSTANT spanned two weak El Niño events, one from late 2004 to early 2005 and one from late 2006 to early 2007, as well as the beginning of a La Niña event in late 2007. However, these events do not dominate the ITF signal during INSTANT.

Under normal conditions, the Indian Ocean is characterized by warmer surface water in the east and cooler surface water in the west. A positive Indian Ocean dipole (IOD) event is defined when the eastern (western) surface waters are anomalously cool (warm) and is usually synchronized with ENSO (Murtugudde et al. 2000; Saji and Yamagata 2006). They are so closely synchronized that some studies have suggested that the IOD exists only as an extension of ENSO (Yu and Lau 2005). Both the ARLINDO and INSTANT periods occurred during significant positive IOD events, which are associated with equatorial winds transporting water to the west, allowing cooler water to upwell along the Java coast. During the 2006 event, the sea surface temperature anomalies remained south of the equator and did not display the westward extension seen in 1997 (Murtugudde et al. 2000; Vinayachandran et al. 2007).

In the period from 1958 through 2007, the correlation coefficient between Niño-3.4 and the dipole mode index (DMI; the index of the IOD) was 0.20. During the ARLINDO period with its strong ENSO event, the correlation coefficient jumped to 0.67. In contrast, the two were uncorrelated during the INSTANT period ($r = 0.11$, $p = 0.54$). It therefore seems possible that this unusual

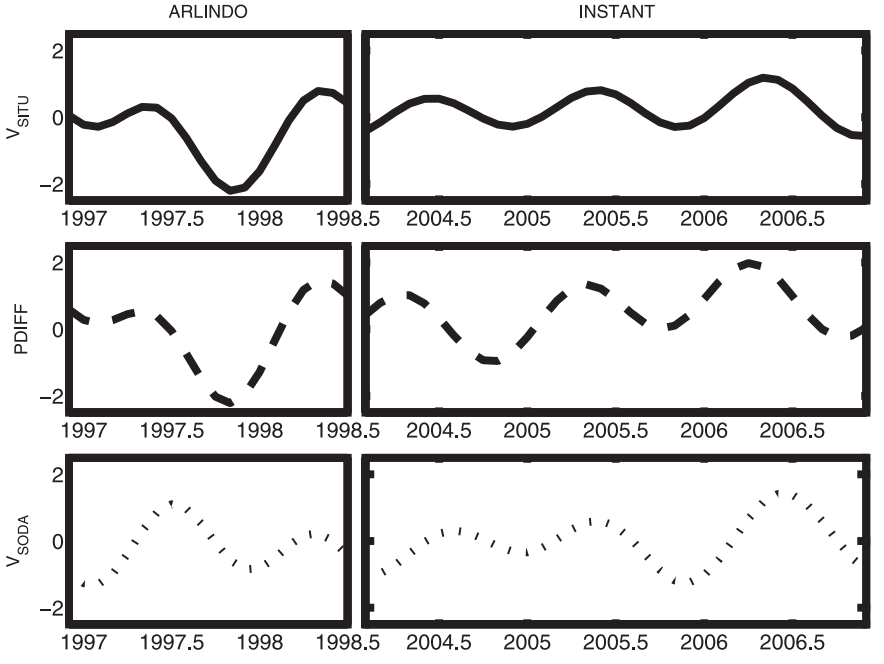

FIG. 4. Long-period (greater than 9 months) components of $\mathbf{V}_{\text{SITU}}$, PDIFF, and $\mathbf{V}_{\text{SODA}}$.

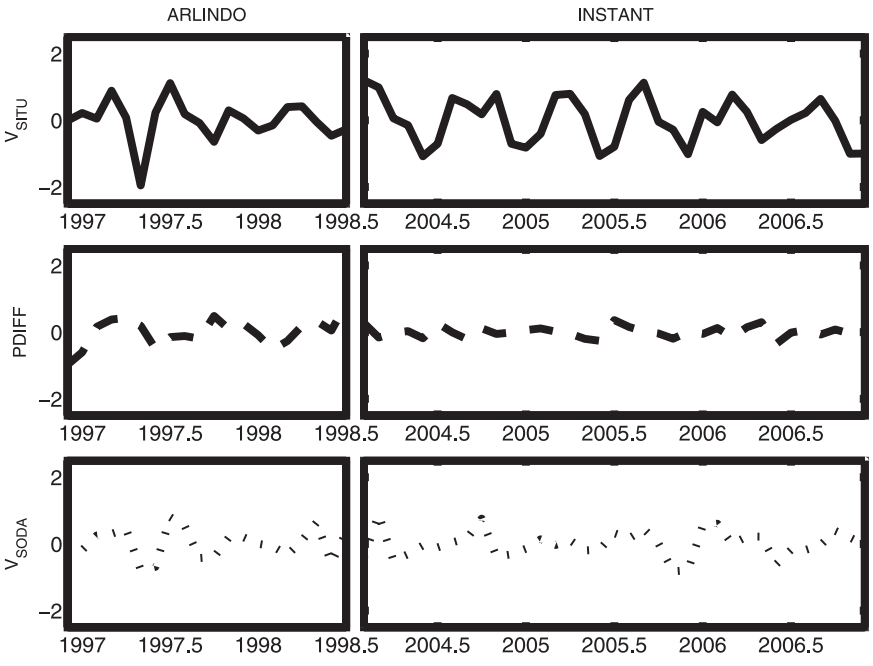

FIG. 5. Short-period (less than 9 months) components of $\mathbf{V}_{\mathrm{SITU}}$, PDIFF, and $\mathbf{V}_{\mathrm{SODA}}$.

lack of synchronicity between the Indian and Pacific Oceans during INSTANT contributed to the difficulty in predicting the low-frequency ITF for that time period, because the low frequency is generally dominated by an ENSO signal that is consistent across the Indian and Pacific Oceans. Although the IOD was in a positive phase during both periods, the IOD signal would have been much weaker than the ENSO signal during ARLINDO and would therefore have been unable to influence the ITF. Because of the short records available, it remains challenging to separate the influences of the IOD and ENSO (Sprintall et al. 2009).

Because the IOD is primarily restricted to the Indian Ocean, its effects would not dominate in the large-scale Pacific Ocean winds and thus would not strongly influence the island rule calculation. A major ENSO event, however, such as the one that occurred in 1997, is associated with surface changes within the South Pacific and along the path used in the island rule calculation (McPhaden 1999).

The apparent disconnect between the SL and deeper layers can be explained by the effects of the local and large-scale wind. When the SL variability and large-scale wind stress are correlated during each observational period, two different patterns emerge. The $\mathrm{SL}_{\mathrm{ARLINDO}}$ is highly correlated with τ_x, the zonal wind stress from SODA (Figs. 6a,b). The pattern of correlation with the zonal wind stress shows three distinct bands, with positive correlation north of the equator, negative correlation from the equator to 20°S, and positive correlation south of 20°S. During INSTANT, the correlations are lower and show less distinct patterns. The only area of high correlation is within the Indonesian Seas and neighboring parts of the Indian and Pacific Oceans: the region that cools with a positive IOD event (Saji et al. 1999). Because it has been shown that the SL is driven by Ekman transport (Wijffels et al. 2008), the lack of predictive skill displayed by PDIFF is expected. The weaker annual signal in $\mathbf{V}_{\mathrm{ARLINDO}}$ than in $\mathbf{V}_{\mathrm{INSTANT}}$ can be attributed to the lack of independent forcing from the local winds if that local signal is damped by the much larger ENSO signal.

During ARLINDO, the pattern of correlation between the TL and the zonal wind stress (Figs. 6c,d) is similar to that of the correlation with the SL, although the zonal structure decreases in the central Pacific Ocean. Unlike the SL, however, the TL correlations during INSTANT remain almost as strong as those during ARLINDO throughout the entire region. Because the flow in this layer is geostrophic (Wijffels et al. 2008), PDIFF successfully estimates its variability.

Potemra and Schneider (2007) performed a similar correlation between zonal wind stress and ITF transport anomalies in an upper 100-m layer and a 100–500-m layer for two coupled models averaged over the length of their runs. For both models, they found that the correlations were different for the two layers, with the upper layer showing a stronger relationship to local and Indian Ocean wind stress (with a 1-month lead) and the middle layer showing a stronger relationship to Pacific

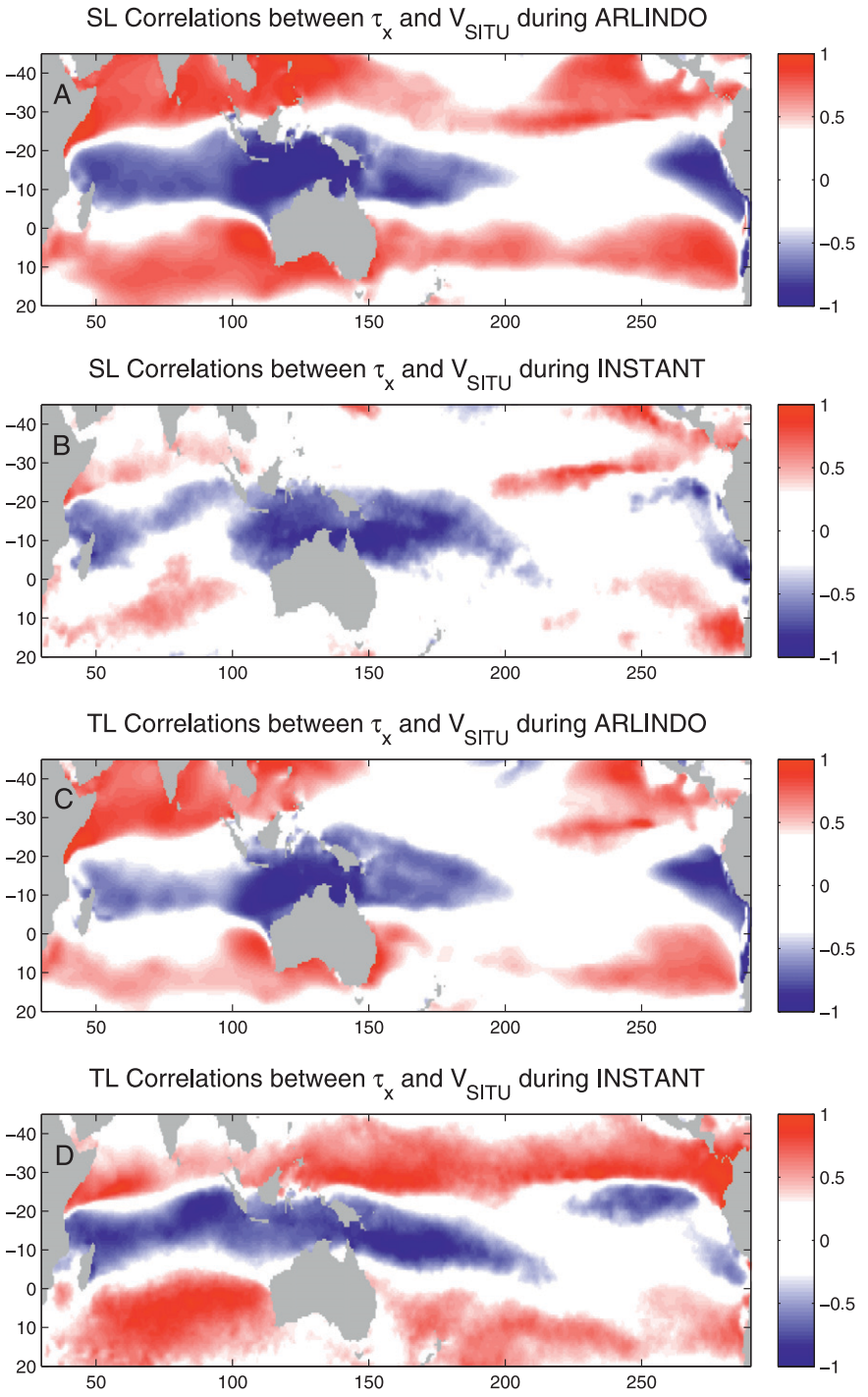

FIG. 6. In situ velocity correlations with τ_x in the SL and TL during ARLINDO and INSTANT. Colors show statistically significant correlations for each observational period.

Ocean wind stress (concurrent and leading), as well as a strong relationship to Indian Ocean wind stress (with a 2–3-month lead). Although that study uses deeper layers than the current study, we also observe that the surface layer maintains a stronger connection to the local wind stress. Although the correlations observed in the current study are much higher than those of Potemra and Schneider (2007), both studies provide evidence of a similar overall scenario of a locally forced surface layer and a remotely forced thermocline layer.

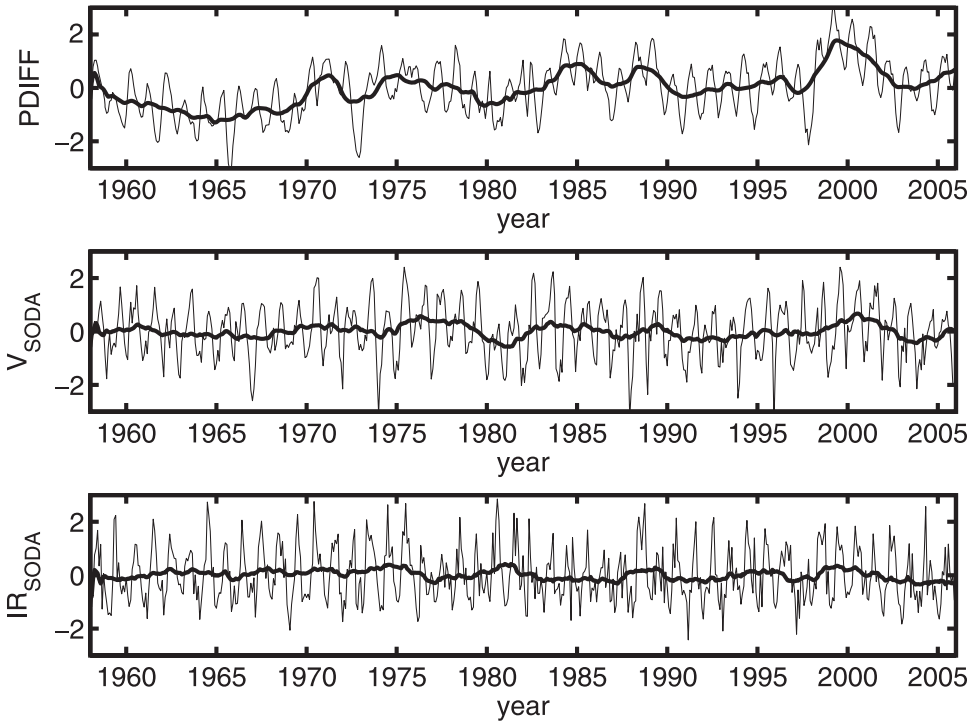

FIG. 7. A 50-yr time series of normalized transport anomalies of PDIFF, $\mathbf{V}_{\mathrm{SODA}}$, and $\mathrm{IR}_{\mathrm{SODA}}$, with a 2-yr running mean.

7. 50-yr ITF time series

As described earlier, the derived time series that were compared with in situ data during 1996–98 and 2004–06—PDIFF and $\mathbf{V}_{\mathrm{SODA}}$—can be extended to a 50-yr record. In addition, the time scale is now sufficiently long for the calculation of the transport using the island rule (Fig. 7).

The island rule was calculated using wind stress form SODA following the formula of Godfrey (1989) along the path shown in Fig. 8:

$$T_{\mathrm{IR}} = \oint \frac{\tau^{l}}{\rho_0 (f_N - f_S)}\, dl, \qquad (2)$$

where, τ^{l} is the component of the wind stress along the counterclockwise path; f_N and f_S are the Coriolis parameters at the northern and southern extents of the integral, respectively; and ρ_0 is the mean density. The resultant transport T is positive in the counterclockwise direction, which in this case is from the Pacific to the Indian Ocean.

Wajsowicz (1993) notes that the island rule calculates an ''ideal'' value for the ITF based on wind stress. This value is subsequently modified by pressure along the western coast of Australia, possibly because of frictional or hydraulic effects, that is in excess of what is needed to balance the wind stress. The island rule can therefore be

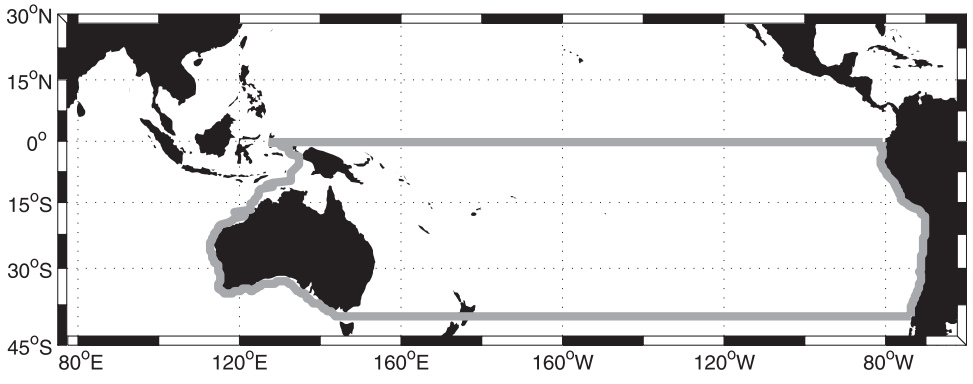

FIG. 8. Map showing the path of the line integral used in the calculation of Godfrey's island rule.

TABLE 4. Correlation coefficients for total and long-period time series of PDIFF, $\mathbf{V}_{SODA}$, and IR_{SODA}.

			Long period only based on cutoff (months)						
		No cutoff	9	12	24	36	48	60	72
PDIFF	$\mathbf{V}_{SODA}$	0.16	0.17	0.21	0.34	0.46	0.55	0.54	0.52
PDIFF	IR_{SODA}	0.06	0.09	0.12	0.19	0.14	−0.02	−0.12	−0.20
IR_{SODA}	$\mathbf{V}_{SODA}$	0.50	0.75	0.50	0.09	0.02	0.08	0.10	0.16

rederived to account for the effects of bottom topography. That study also notes that this modified island rule is valid at interannual and longer time scales. Given that the available observational studies are too short to produce robust interannual data, we do not compare any island rule results to the observational time series but instead compare it to the longer, SODA-derived time series.

Among the 50-yr time series, the strongest correlation is between the island rule IR_{SODA} and $\mathbf{V}_{SODA}$ (Table 4). Limiting the comparison to only low frequencies further improves the correlation, which is a stronger correlation than the one seen in previous work comparing the island rule and ITF transport from within a particular model (Humphries and Webb 2008). PDIFF is correlated with $\mathbf{V}_{SODA}$ but not with IR_{SODA}. When only low frequencies are considered, all of the time series are well correlated with each other; when only high frequencies are considered, only IR_{SODA} and $\mathbf{V}_{SODA}$ are correlated (not shown; $r = 0.18$). However, when the time series are filtered to isolate periods longer than 9 months, we see that the correlation between PDIFF and $\mathbf{V}_{SODA}$ improves as the cutoff period is lengthened to 4 yr. The correlation between PDIFF and IR_{SODA} peaks when periods shorter than 2 yr are considered. However, the highest correlation between IR_{SODA} and $\mathbf{V}_{SODA}$ is achieved when the cutoff period remains at 9 months.

To explain these correlations, a fast Fourier transform (FFT) was used to examine the dominant frequencies of all four time series. Figure 9 shows frequencies between 2 and 16 yr. This excludes the strong annual and semiannual

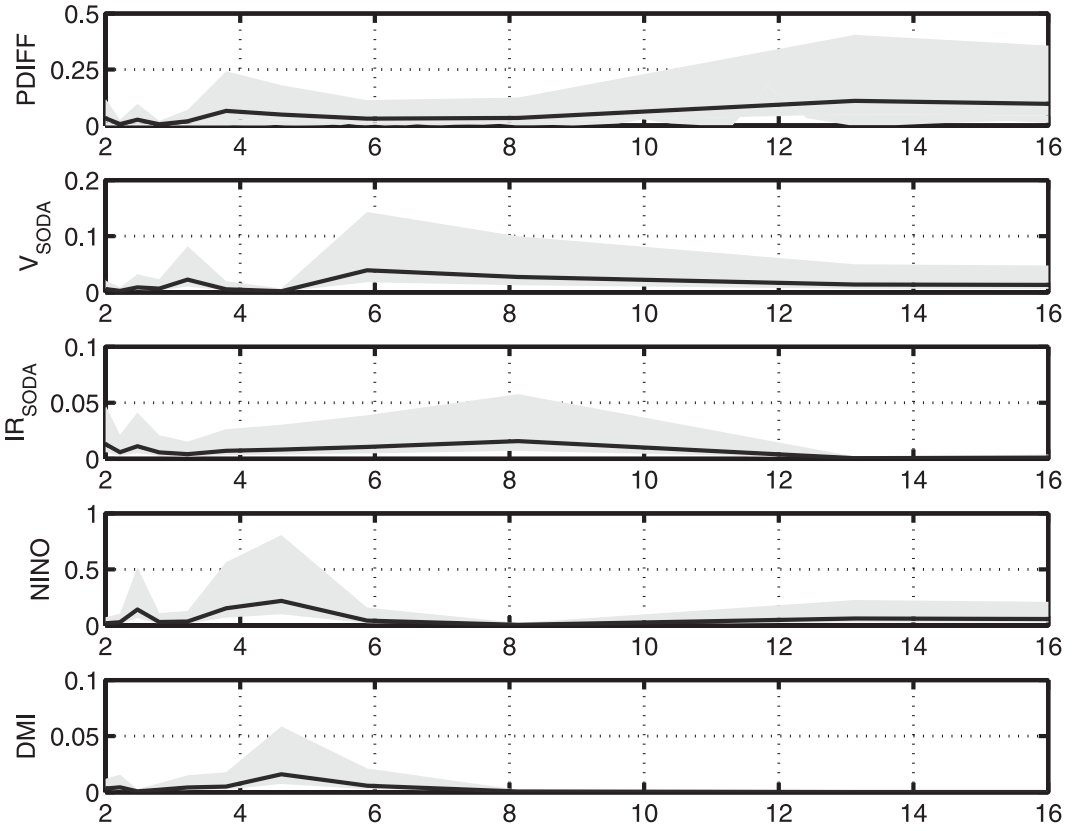

FIG. 9. Frequency spectra for periods of 2 through 16 yr of (top)–(bottom) PDIFF, $\mathbf{V}_{SODA}$, IR_{SODA}, Niño-3.4, and DMI.

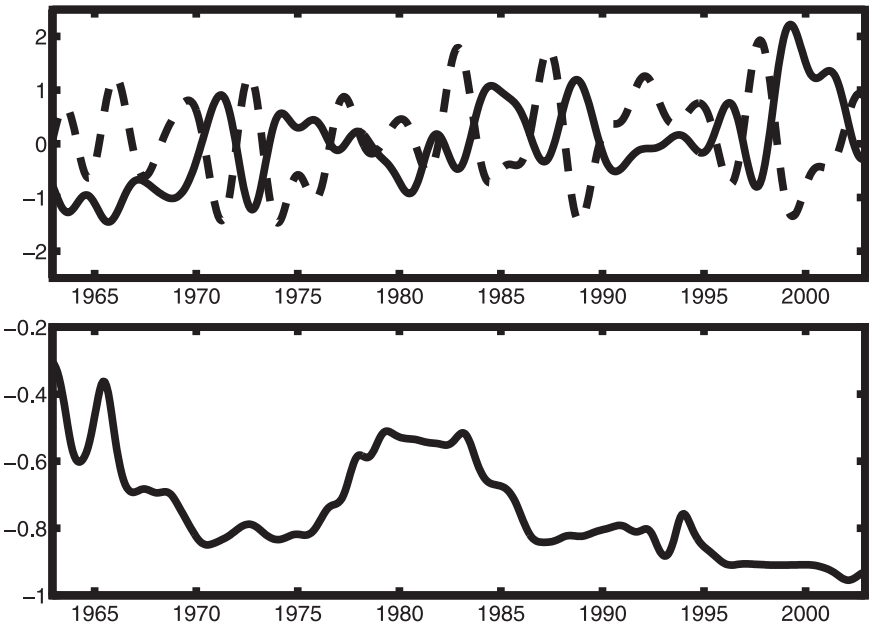

FIG. 10. (top) PDIFF (solid) and Niño-3.4 (dashed) frequencies below 2 yr and (bottom) the 10-yr running correlation between PDIFF and Niño-3.4.

cycles of IR_{SODA} and $\mathbf{V}_{SODA}$. There were no significant peaks at periods above 16 yr. On time scales longer than 2 yr, many of the dominant frequencies can be found in the Niño-3.4 and DMI indices (Fig. 9, bottom). Only PDIFF displays significant power within the 4–5-yr peak shown by Niño-3.4. The DMI does not have any unique peaks with corresponding peaks in the time series, but it does show a peak within the main Niño-3.4 frequency band. This suggests that if there is a relationship between the IOD and the ITF within the Makassar Strait, it is not wholly separate from the relationship between ENSO and the ITF at periods longer than 2 yr.

PDIFF, IR_{SODA}, and the composite time series all show a negative correlation with Niño-3.4, meaning that El Niño (La Niña) events are correlated with less (more) throughflow, as expected. The only derived measure of ITF variability that does not show any relationship with Niño-3.4 is $\mathbf{V}_{SODA}$. However, when the time series are again decomposed into high and low frequencies, they all show correlations between their low-frequency components and Niño-3.4. The correlation between PDIFF and IRSODA improves as progressively lower frequencies are considered.

Because PDIFF showed the highest overall skill in the estimation of in situ variability, its relationship with Niño-3.4 is further investigated. When only frequencies below 2 yr are considered, the overall correlation coefficient between the PDIFF and Niño-3.4 is −0.52. However, that value varies considerably over time (Fig. 10). When the correlation is computed for continuously overlapping 10-yr periods, the correlation coefficient ranges from −0.30 to −0.95. The decadal variation shows the lowest correlation at the start of the record, which could be the result of insufficient data in the SODA reanalysis. The correlation improves during the 1970s, then it reduces through much of the 1980s. After the 1986/87 El Niño event, the correlation remains high through the end of the record. On average, the correlation between the ITF and the Niño-3.4 index is higher when the index is positive (−0.39) than when the index is negative (−0.24), implying a stronger ITF response to El Niño events than to La Niña events.

8. Conclusions

The comparison between two different SODA-based estimates of the Indonesian throughflow variability with observational data from two periods provides confidence that a long-term ITF time series can be generated from reanalysis data. Particularly effective is the interocean pressure difference method PDIFF for long-period variability. The ITF can be successfully monitored by large-scale hydrological data, which is routinely collected and for which there is a much richer archival dataset than in situ velocity measurements. A more precise conversion of the interocean pressure gradient to the ITF profile based on hydrographic data would require further consideration of the dissipation of energy resulting from friction and transfer to eddy kinetic energy. In addition, although the Makassar Strait is the primary pathway for

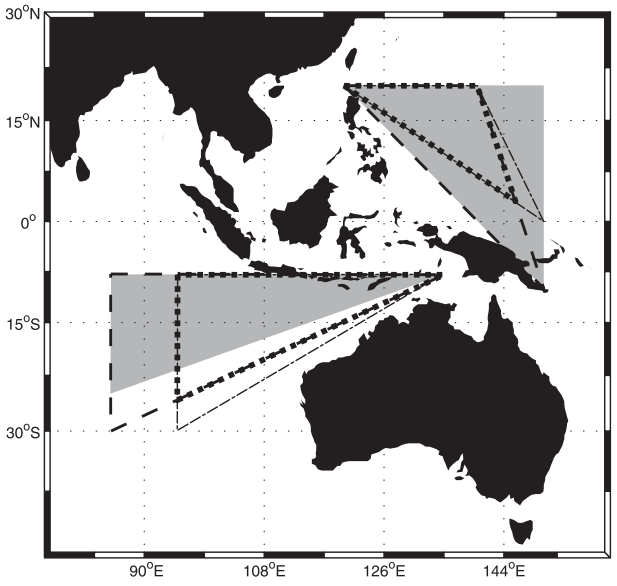

FIG. A1. Inflow and outflow triangle areas used to test the sensitivity of the pressure difference calculation.

the ITF, the inclusion of data from the Lifamatola Strait, located to the east of Sulawesi, particularly for subthermocline levels, might present a fuller picture. Furthermore, this method of calculating ITF variability by using pressure differences suggests the possibility of a paleoceanographic study using coral isotopes as proxies for ocean temperature and density data in the ITF inflow and outflow regions.

Acknowledgments. The INSTANT data analysis is funded by National Science Foundation Grant OCE 07-25935. We thank Janet Sprintall and James Carton for helpful discussions and two anonymous reviews for their comments.

APPENDIX

Sensitivity Test for Pressure Difference Calculation

Figure A1 shows various triangle extents that were used to test the sensitivity of the pressure difference calculation [Eq. (1)] to the choice of inflow and outflow areas used. For each triangle, the average density anomaly (1000 kg m^{-3} − 1000) was calculated and compared to the density anomalies of the triangles used in this study (shown in gray in Figure A1). For both the inflow and outflow regions, the differences in density anomalies among the different triangles in each region were all below 2.1%, with an average of 0.23% in the Pacific and 0.36% in the Indian Ocean. These slight variations are approximately constant in time. Within the Pacific inflow boxes, they are approximately equally distributed with depth. Within the Indian Ocean outflow triangle, the maximum differences are within the surface layer, but these differences average less than 1%.

From this test, we conclude that the pressure difference calculation is not very sensitive to the choice of inflow and outflow regions, provided that they are adjacent to the Indonesian Seas. On the Pacific side, we see that the inclusion of a small amount of South Pacific water does not significantly change the overall characteristics of the inflow area. Expanding the triangles zonally had little effect, because the ocean tends not to vary zonally away from littoral regions. Within the Indian Ocean, the biggest changes were found when the triangle extended far south and west. We therefore conclude that inclusion of water from the southern Indian Ocean, perhaps via the Leeuwin Current, changes the results slightly.

REFERENCES

Andersson, H. C., and A. Stigebrandt, 2005: Regulation of the Indonesian throughflow by baroclinic draining of the North Australian Basin. *Deep-Sea Res. I,* **52,** 2214–2233.

Burnett, W. H., V. M. Kamenkovich, A. L. Gordon, and G. L. Mellor, 2003: The Pacific/Indian Ocean pressure difference and its influence on the Indonesian Seas circulation: Part I—The study with specified total transports. *J. Mar. Res.,* **61,** 577–611.

Carton, J. A., and B. S. Giese, 2008: A reanalysis of ocean climate using SODA. *Mon. Wea. Rev.,* **136,** 2999–3017.

——, G. Chepurin, X. Cao, and B. Giese, 2000a: A Simple Ocean Data Assimilation analysis of the global upper ocean 1950–95. Part I: Methodology. *J. Phys. Oceanogr.,* **30,** 294–309.

——, ——, and ——, 2000b: A Simple Ocean Data Assimilation analysis of the global upper ocean 1950–95. Part II: Results. *J. Phys. Oceanogr.,* **30,** 311–326.

Clark, A. J., and X. Liu, 1994: Interannual sea level in the northern and eastern Indian Ocean. *J. Phys. Oceanogr.,* **24,** 1224–1235.

Duchon, C. E., 1979: Lanczos filtering in one and two dimensions. *J. Appl. Meteor.,* **18,** 1016–1022.

Ffield, A., and A. L. Gordon, 1992: Vertical mixing in the Indonesian Thermocline. *J. Phys. Oceanogr.,* **22,** 184–195.

Godfrey, J. S., 1989: A Sverdrup model of the depth-integrated flow for the World Ocean allowing for island circulations. *Geophys. Astrophys. Fluid Dyn.,* **45,** 89–112.

Gordon, A. L., 2005: Oceanography of the Indonesian Seas and their throughflow. *Oceanography,* **18,** 14–27.

——, and R. A. Fine, 1996: Pathways of water between the Pacific and Indian oceans in the Indonesian Seas. *Nature,* **379,** 146–149.

——, C. F. Giulivi, and A. G. Ilahude, 2003: Deep topographic barriers within the Indonesian seas. *Deep-Sea Res.,* **50,** 2205–2228.

——, R. D. Susanto, A. Ffield, B. A. Huber, W. Pranowo, and S. Wirasantosa, 2008: Makassar Strait throughflow, 2004 to 2006. *Geophys. Res. Lett.,* **35,** L24605, doi:10.1029/2008GL036372.

Humphries, U. W., and D. J. Webb, 2008: On the Indonesian Throughflow in the OCCAM 1/4 degree ocean model. *Ocean Sci.,* **4,** 183–198.

Kamenkovich, V. M., W. H. Burnett, A. L. Gordon, and G. L. Mellor, 2003: The Pacific/Indian Ocean pressure difference and its influence on the Indonesian Seas circulation: Part II—The study with specified sea-surface heights. *J. Mar. Res.,* **61,** 613–634.

Koch-Larrouy, A., G. Madec, P. Bouruet-Aubertot, T. Gerkema, L. Bessières, and R. Molcard, 2007: On the transformation of Pacific Water into Indonesian Throughflow Water by internal tidal mixing. *Geophys. Res. Lett.,* **34,** L04604, doi:10.1029/2006GL028405.

McPhaden, M. J., 1999: Genesis and evolution of the 1997-98 El Niño. *Science,* **283,** 950–954.

Meyers, G., 1996: Variation of Indonesian throughflow and the El Niño–Southern Oscillation. *J. Geophys. Res.,* **101,** 12 255–12 263.

——, R. H. Bailey, and A. P. Worby, 1995: Geostrophic transport of Indonesian throughflow. *Deep-Sea Res.,* **42,** 1163–1174.

Murtugudde, R., J. P. McCreary Jr., and A. J. Busalacchi, 2000: Oceanic processes associated with anomalous events in the Indian Ocean with relevance to 1997–1998. *J. Geophys. Res.,* **105,** 3295–3306.

Potemra, J. T., 1999: Seasonal variations of upper ocean transport from the Pacific to the Indian Ocean via Indonesian straits. *J. Phys. Oceanogr.,* **29,** 2930–2944.

——, 2005: Indonesian Throughflow transport variability estimated from satellite altimetry. *Oceanography,* **18,** 98–107.

——, and N. Schneider, 2007: Interannual variations of the Indonesian throughflow. *J. Geophys. Res.,* **112,** C05035, doi:10.1029/2006JC003808.

——, R. Lukas, and G. T. Mitchum, 1997: Large-scale estimation of transport from the Pacific to the Indian Ocean. *J. Geophys. Res.,* **102,** 27 795–27 812.

——, S. L. Hautala, J. Sprintall, and W. Pandoe, 2002: Interaction between the Indonesian Seas and the Indian Ocean in observations and numerical models. *J. Phys. Oceanogr.,* **32,** 1838–1854.

RDI, 2001: Acoustic Doppler current profiler principles of operation: A practical primer. RD Instruments, 50 pp.

Saji, N. H., and T. Yamagata, 2006: Tropical Indian Ocean variability in the IPCC twentieth-century climate simulations. *J. Climate,* **19,** 4397–4417.

——, B. N. Goswami, P. N. Vinayachandran, and T. Yamagata, 1999: A dipole mode in the tropical Indian Ocean. *Nature,* **401,** 360–363.

Song, Y. T., 2006: Estimation of interbasin transport using ocean bottom pressure: Theory and model for Asian marginal seas. *J. Geophys. Res.,* **111,** C11S19, doi:10.1029/2005JC003189.

Sprintall, J., and Coauthors, 2004: INSTANT: A new internations array to measure the Indonesian Throughflow. *Eos, Trans. Amer. Geophys. Union,* **85,** doi:10.1029/2004EO390002.

——, S. E. Wijffels, R. Molcard, and I. Jaya, 2009: Direct estimates of the Indonesian Throughflow entering the Indian Ocean: 2004–2006. *J. Geophys. Res.,* **114,** C07001, doi:10.1029/2008JC005257.

Susanto, R. D., and A. L. Gordon, 2005: Velocity and transport of the Makassar Strait throughflow. *J. Geophys. Res.,* **110,** C01005, doi:10.1029/2004JC002425.

van Aken, H. M., I. Brodjonegoro, and I. Jaya, 2009: The deep-water motion through the Lifamatola Passage and its contribution to the Indonesian throughflow. *Deep-Sea Res. I,* **56,** 1203–1216, doi:10.1016/j.dsr.2009.02.001.

Vinayachandran, P. N., J. Kurian, and C. P. Neema, 2007: Indian Ocean response to anomalous conditions in 2006. *Geophys. Res. Lett.,* **34,** L15602, doi:10.1029/2007GL030194.

Wajsowicz, R. C., 1993: The circulation of the depth-integrated flow around an island with application to the Indonesian Throughflow. *J. Phys. Oceanogr.,* **23,** 1470–1484.

Waworuntu, J. M., S. L. Garzoli, and D. B. Olson, 2001: Dynamics of the Makassar Strait. *J. Mar. Res.,* **59,** 313–325.

Wijffels, S. E., G. Meyers, and J. S. Godfrey, 2008: A 20-yr average of the Indonesian Throughflow: Regional currents and the interbasin exchange. *J. Phys. Oceanogr.,* **38,** 1965–1978.

Wyrtki, K., 1987: Indonesian through flow and the associated pressure gradient. *J. Geophys. Res.,* **92,** 12 941–12 946.

Yu, J. Y., and K. M. Lau, 2005: Contrasting Indian Ocean SST variability with and without ENSO influence: A coupled atmosphere-ocean GCM study. *Meteor. Atmos. Phys.,* **90,** 179–191.